Optimal Geometry and Materials for Nanospacecraft Magnetic Damping Systems

F. SANTONI
M. L. BATTAGLIERE
University of Rome "La Sapienza",
Rome, Italy

F. FIORILLO
E. FERRARA
Istituto Nazionale di Ricerca Metrologica,
Torino, Italy

A magnetic damping system for nanospacecraft attitude stabilization is proposed, based on the use of thin strips of amorphous Fe-B-Si soft magnetic ribbons. The size, number, and location of the strips is optimized, and a predictive formulation is provided. The main result of ground tests, comparing the performance of several soft magnetic materials, is that suitably heat-treated amorphous ribbons provide the best loss performance in the whole range of magnetic fields expected in orbit.

Manuscript received March 31, 2013; revised April 1, 2014; released for publication June 26, 2014.

DOI. No. 10.1109/TAES.2014.130218.

Refereeing of this contribution was handled by S. Nakasuka.

Authors' addresses: F. Santoni, M. L. Battagliere, University of Rome "La Sapienza," Dipartimento di Ingegneria Astronautica Elettrica ed Energetica (DIAEE), Via Salaria 851, Rome, 00138 Italy, E-mail: (fabio.santoni@uniroma1.it); F. Fiorillo, E. Ferrara, Istituto Nazionale di Ricerca Metrologica, Torino, 10135 Italy.

I. INTRODUCTION

Magnetic damping systems, based on the magnetic hysteresis loss of soft magnetic materials, have been used since the very early space missions in passive attitude stabilization systems [1, 2, 3]. Renewed interest in these systems has been generated by the nanosatellites appearing on the space market and the advent of small university satellites, such as CubeSats [4–8]. Though state-of-the-art attitude control systems benefit from electronic components miniaturization, while sophisticated sensors and control algorithms are available for nanosatellites in the range of 1-kg total mass [9], many nanosatellite missions have loose requirements in terms of spacecraft attitude pointing and maneuvering. In this class of satellites, passive attitude stabilization systems can be effective, while simplifying the onboard system design, realization, and reliability [10]. An effective dissipation route, suitable for low Earth orbiting spacecraft, is the magnetic hysteresis, not requiring moving parts, liquids, or pressurized tanks and guaranteeing a sufficient level of dissipation under the typical slow motion of passively stabilized spacecraft. Despite the simplicity of the basic physical dissipation phenomenon, correct sizing of the system is not trivial. Because we necessarily need to use open samples, we must face the complications arising from the nonuniform nature of the demagnetizing field, as imposed by the nonellipsoidal shape of the magnetized bars and the difficult modeling of the bar-to-bar magnetic interactions. This is complicated further by the irregularities in the satellite attitude motion, which reflect in nonsymmetrical hysteresis loops and complex magnetic histories suffered by the orbiting soft magnetic rods. Experience in orbit of UNISAT-3 showed that the satellite oscillation amplitude around the geomagnetic field was of the order of 30° [11], far from the expected nominal behavior. Unexpected performance in orbit was observed also in the Delfi-C3 mission [12], in which PERMENORM 5000H2 (Ni-Fe alloy) permeable rods were used [13]. The O/OREOS mission in-orbit measurements revealed a much longer settling time of the attitude motion, with respect to numerical simulations, as reported in [14].

Hence, even if the magnetic hysteresis energy dissipation concept is well known, there are still open issues and room for further optimization and enhancement of the performance of magnetic damping systems.

Design procedures for evaluation of permanent magnet dipole, depending on the system parameters, such as satellite inertia, orbital height, and inclination, can be found, for example, in [15–18].

In this paper, we concentrate on the performance of the energy dissipation system based on soft magnetic bars, within the geometrical constraints imposed by typical nanospacecraft size. With the external geometry fixed, we devise the combination of material and geometrical layout of the permeable rods leading to maximum dissipated energy per unit volume in the low Earth orbit magnetic environment.

The energy dissipation dramatically depends of the ability of the permeable bars to magnetize to an effective extent under the Earth's magnetic field experienced in orbit. This results from a complex combination of 1) the intrinsic magnetic properties of the soft magnetic material, 2) the geometrical layout of the bars, including the shape of the single bar and the way the bars are arranged one with respect to another, 3) the irregular magnetic histories imposed on the rods by the satellite attitude motion, resulting in asymmetric hysteresis loops.

Concerning point 1), the material performance could, in principle, be evaluated exploiting the data provided by the manufacturer. However, these data, obtained using closed magnetic circuits, are often incomplete, while having an intrinsic character, and one must face the difficult problem of predicting the material behavior in a system made of open and interacting samples. Actually, a range of values for the magnetization level reached in satellite damping systems is given in the literature. Depending on the rod geometry, material, and treatment, magnetization levels of the order of 0.1 T, 0.7 T, 0.015 T, 0.14 T, 0.07 T, and 0.15 T are reported in [1, 3, 14, 17, 18, 19], respectively. This shows that the "optimal" material choice, clearly related to the overall geometry of the system, is ill defined and needs further investigation.

Spacecraft magnetic damping systems are traditionally based on Ni-Fe alloys [1, 2, 13]. Fe-Si alloys were tested on the ground in the material selection process for the TRANSIT satellite [1]. In this paper, we analyze the performance of innovative magnetic materials and the amorphous Fe-B-Si alloys and compare them with that of the conventional Ni-Fe and Fe-Si alloys (Section III).

Concerning point 2), although the demagnetizing effect of isolated elongated bars has been investigated in detail in the literature and approximate analytical descriptions have been provided for both fluxmetric and magnetometric demagnetizing factors [20, 21, 22], useful for predicting the resulting energy dissipation, design procedures or experimental data for nanospacecraft multiple soft magnetic rod systems are hardly available. In nanospacecraft applications, where the bar length is severely limited, the dissipation offered by a single magnetic rod may not be sufficient for achieving the necessary level on energy dissipation and a many-bar system should be employed. Pioneering papers, such as [1, 2, 3], refer to large satellites, and because the rod size is a key factor in the energy dissipation performance, their results are not directly applicable to nanospacecrafts. A magnetic damping system for nanospacecraft, based on two arrays of three cross-section mumetal bars (1 mm $\times$ 1 mm) arranged on two orthogonal planes is analyzed in [15] and [23]. The bar-to-bar distance is selected, assuming that the mutual interaction brings about a 12.5% reduction in energy dissipation, when such a distance is 20% of the bar length, while it can be neglected when it becomes larger than 30% of the bar length.

In this paper, we focus our attention on magnetically stabilized nanospacecrafts, with a size in the 10- to 20-cm range, endowed with planar arrays of dissipating soft magnetic strips, without a priori limitations in the number of strips and their mutual distance. After an extensive testing campaign on several geometrical configurations, we show that under appropriate simplifying assumptions, a synthetic analytical model of the overall permeable rod system dissipated energy can be built. This is based on the introduction of a cumulative demagnetization factor for all the bars, extending the results known for isolated bars. In this model, the demagnetizing effect is described by two empirical parameters only, which lump the complex combination of the demagnetizing effect and the strip-to-strip magnetic interactions. It is recognized that due to the open geometry, the ensuing demagnetizing effect, and bar-to-bar magnetic interactions, the material magnetization is not homogeneous. Consequently, its measured variation along the strip axis is empirically modeled to predict the overall system dissipation. Although this model is valid, whatever the employed material, the array configuration and the magnetizing field intensity expected in low Earth orbit, we experimentally evaluated the model parameters for arrays of 10- and 20-cm-long strips. Thus, based on the measured properties of the materials, namely, normal magnetization curve and hysteresis energy loss, the combination of strip thickness and strip-to-strip distance leading to maximum dissipated energy per magnetic cycle under a given alternating field is provided (Sections IV and V).

The study is completed (Section VI) by the experimental analysis of the effect of a bias by an external magnetic field, such as the one generated by the pivoting permanent magnet or other magnetic or electric equipment onboard the satellite. It is verified that the dissipating performance of the strip array is not significantly affected by a magnetic field orthogonal to the plane of the array, which is the case for a pivoting magnet centered with respect to this plane and pointing normally to it.

Concerning point 3), the expected performance in orbit of the optimal bar configuration is evaluated by numerical simulations for both the innovative Fe-B-Si amorphous strips and the conventional Ni-Fe bars. Due to the large demagnetizing effect of the dissipating array, the magnetic hysteresis loops measured on the overall system show a pseudolinear behavior. This allows one to use a simplified semianalytical model for the magnetization of the strips, which is useful for the dynamical simulation of the spacecraft attitude motion, as suggested in [14, 24]. Numerical simulations confirm the superior performance of the amorphous alloys and the proposed geometrical arrangement with respect to the Ni-Fe alloys. Relevant improvements are obtained both in terms of attitude acquisition time and in the stabilized angular motion amplitude.

The main intended contributions of this work paper can then be summarized in 1) the introduction of an innovative material (Fe-B-Si alloys) for the permeable rods; 2) the introduction and the analytical modeling of the cumulative demagnetizing factor; 3) the use of the

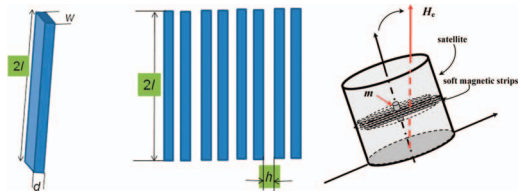

Fig. 1. (Left) Soft magnetic strip. (Middle) Strip array. (Right) Schematic view of strip array and pivoting permanent magnet oscillating in Earth's magnetic field $\boldsymbol{H}_e$.

newly developed demagnetization model for the evaluation of the cumulative dissipated energy of a magnetic strip array; 4) the experimental evaluation of the effect of a bias field on the strip array dissipation performance; and 5) the evaluation of the performance in orbit by numerical simulations.

II. EXPERIMENTAL CAMPAIGN RATIONALE

A natural and flexible arrangement for the energy dissipating system is the one offered by an array of soft magnetic strips, conveniently fastened to the satellite (see Fig. 1). The strip geometry provides magnetic response only for the component of the environmental field directed along the strip axis. Consequently, if the axis of the small cylindrical permanent magnet used to align the satellite with Earth's magnetic field is orthogonal to the plane of the array, its dipolar field is equally orthogonal to the strip surface and is thereby expected to negligibly interfere with the magnetization process in the soft magnets.

The following main parameters of the problem are identified: 1) the magnetic properties of the selected soft magnetic material; 2) the geometrical features of the individual strips; 3) the mutual arrangement of the strips in the array; and 4) the range of envisaged peak values of the Earth field component along the strip axis. One should further take into account the effect of the spurious field originating from the pivoting permanent magnet, the hysteresis behavior in the presence of a field bias (with the material performing minor asymmetric hysteresis loops), and the torque applied at any instant of time on the array of oscillating strips by the component of the Earth field orthogonal to the strip axis.

In the present investigation, we have carried out a comprehensive experimental and theoretical analysis of the energy dissipation in arrays of soft magnetic strips, subjected to slow (quasistatic) cyclic variation of an external field, emulating the actual magnetic environment of small orbiting satellites. The experimental setup is described in detail in [25]. A method for predicting the energy loss in arrays of soft magnetic strips, subjected to these quasistatic alternating magnetic fields of strength ranging between 2 A/m and 40 A/m and for devising the strip arrangement leading to maximum dissipation, is worked out. Six different heat-treated soft magnetic materials have been considered, whose quasistatic behavior (normal magnetization curve, hysteresis loop, and energy loss) has been measured up to magnetic saturation. The evolution of magnetic hysteresis loops and losses with the peak field strength has then been experimentally obtained in actual arrays made of 5.4-mm-wide and 20.3-μm-thick $Fe_{78}B_{13}Si_9$ strips, annealed at 325°C under saturating longitudinal field. Two differently sized strip arrays (200 mm $\times$ 200 mm and 100 mm $\times$ 100 mm) have been tested as a function of the strip-to-strip distance h. The dependence of the energy loss on h under the given applied alternating field strength passes through a maximum value and can be quantitatively predicted by explicitly expressing the magnetostatic interaction of the regularly aligned strips, the preemptive knowledge of the intrinsic magnetic behavior of the material (i.e., the normal magnetization curve, and the quasistatic loss versus peak polarization) being required. Exploiting these experiments, the energy dissipation on arrays obtained with different types of soft magnets and strip cross-sectional areas are predicted. It is concluded that conveniently annealed amorphous Fe-based ribbons provide the best response in terms of versatility and maximum loss under the range of oscillating field amplitudes expected to arise in orbiting satellites. This conclusion takes into account both the decay of the magnetization occurring from center to end in the strips and the role of a bias field.

The demagnetizing field brings about a good simplification in treating the magnetic response of the strip array. It leads, in particular, to quasilinear dependence of the magnetization on the oscillating applied field strength, the resulting hysteresis loop combining low coercivity with low remanence. This permits one to make the simplifying and important assumption of history-independent magnetic behavior of the material.

The study is completed by the experimental evaluation of the following effects: 1) role of a DC bias field generated by onboard devices. For a given oscillating field strength, lower magnetization swing (i.e., lower loss) is engendered by increasing bias. 2) Effect of the stray field generated by the pivoting hard magnet (see Fig. 1). It may provide further disturbance to the magnetization process in the soft strips, tending again to decrease the magnetic loss.

III. THE MATERIALS AND THEIR CHARACTERIZATION

The requirement of maximum parasitic torque by the employed soft magnetic materials in the expected range of field strength values (maximum around 40 A/m) calls for the somewhat contrasting requirements of high losses and high magnetic softness. The latter is important for providing maximum magnetic response in this range of applied fields. On the other hand, too soft a magnet may give rise to little dissipation, because the energy loss per cycle is proportional to the coercive field, and one could not optimally cover the whole envisaged field range. A low saturation magnetization, such as the one associated with Fe-Ni or Co-based amorphous alloys, can be an additional drawback.

TABLE I
Parameters of the Investigated Soft Magnetic Materials

	J_s (T)	T_c (°C)	T_a (°C)	H_c (A/m)	d (μm)	w (mm)
$Fe_{14}Ni_{77}Mo_4Cu_5$ (mumetal)	0.78	400	1100	3.45	1000	1.0
GO Fe-(3 wt%)Si	2.02	750	780	7.3	100	5.0
$Fe_{78}B_{13}Si_9$	1.55	415	325	3.75	20.3	5.4
$Fe_{78}B_{13}Si_9$	1.55	415	360	1.75	20.0	5.0
$Fe_{78}B_{13}Si_9$	1.55	415	400	1.65	20.0	5.0
$Fe_{80}B_{10}Si_{10}$	1.60	395	380	3.5	20.0	10.0

[a] $J_s \equiv$ saturation polarization; $T_c \equiv$ Curie temperature; $T_a \equiv$ annealing temperature; $H_c \equiv$ coercive field; $d \equiv$ strip sample thickness; $w \equiv$ strip sample width. The amorphous ribbons have all been annealed under a longitudinally directed saturating magnetic field.

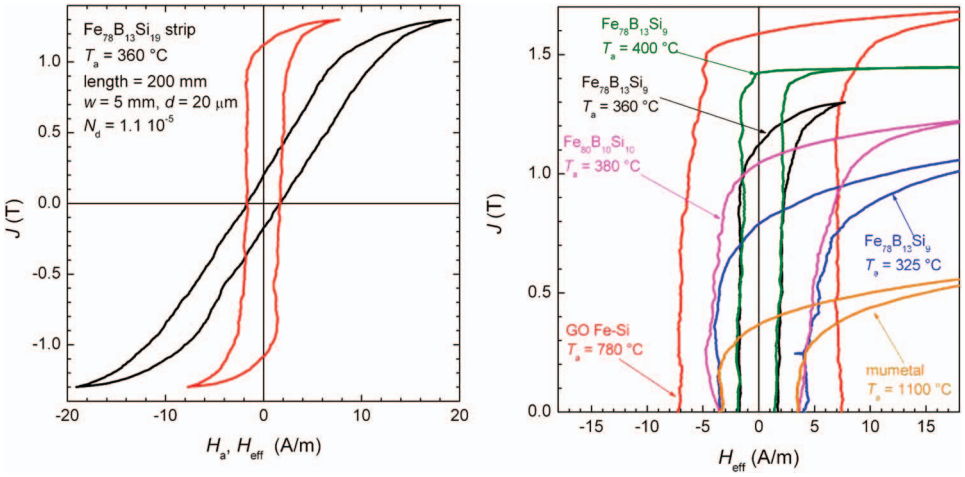

Fig. 2. (Left) Major hysteresis loop in amorphous $Fe_{78}B_{13}Si_9$ strip sample. Intrinsic loop (red dashed line) is obtained from measured loop (black solid line) after correction for demagnetizing field ($H_{eff} = H_a - H_d = H_a - (N_d/\mu_0)J$). (Right) Comparison of intrinsic major loops obtained in investigated soft magnetic alloys.

A fundamental role in the preemptive assessment of the material behavior is additionally played by the demagnetizing effect, which is made relevant by the strip-to-strip magnetostatic interaction. The demagnetizing field, expressed in scalar form, is $H_d = -1 (N_d/\mu_0) J$, where N_d is the collective fluxmetric demagnetizing factor, μ_0 is the magnetic constant, and J is the magnetic polarization.

We have considered the following soft magnetic alloys: 1) $Fe_{14}Ni_{77}Mo_4Cu_5$ (mumetal); 2) grain-oriented (GO) Fe-(3wt%)Si (M2H type); 3) $Fe_{78}B_{13}Si_9$ amorphous alloy; and 4) $Fe_{80}B_{10}Si_{10}$ amorphous alloy. Their intrinsic properties, the sample geometries, and the annealing temperatures are given in Table I. Samples have been prepared as strips (100 mm and 200 mm long), cut either from a parent sheet (mumetal and GO Fe-SiFe) or from the as-quenched amorphous ribbons. The mumetal strips, having a cross-sectional area of 1 mm $\times$ 1 mm, were annealed at 1100°C and rapidly cooled through the ordering region. The GO Fe-Si strips were chemically thinned down to a minimum thickness $d = 100$ μm, starting from the original 300-μm-thick sheet, and stress relieved at 780°C. The amorphous Fe-based alloys, obtained by rapid solidification as either 5-mm- or 10-mm-wide, 20-μm-thick ribbons, were annealed under a saturating longitudinally applied field at temperatures ranging between 325°C and 400°C—the higher the temperature, the softer the final material. It is important to stress that there is no complete freedom of choice regarding the strip geometry: GO Fe-Si sheets cannot be reasonably thinned below 100 μm without impairment of their soft properties, and mumetal ribbons are typically delivered with a minimum thickness around 50 μm, while the Fe-based amorphous alloys are obtained with thickness around 20 μm. This engenders some limitation on the geometry of the dissipating strip arrays.

Initial magnetization curve and hysteresis loops were obtained up to technical saturation under quasistatic excitation ($f = 1$ Hz) on single strips (200 mm long), using a digital hysteresis graph. The induction was measured by means of a narrow pickup coil localized at the center of the strip. The strip arrays were tested by placing them at the center of a solenoid (150 cm long and 35 cm diameter). A detailed description of the experimental setup and measurement procedure can be found in [26]. The decay of the magnetization from the center point to the end of the strip was separately determined by placing the pickup coil at different positions along the strip length. Such a decay, eventually measured on the strip array, must be taken into account in the prediction of the energy losses. For the time being, our discussion will refer to the array midline. Fig. 2(Left) shows an example of DC major loop

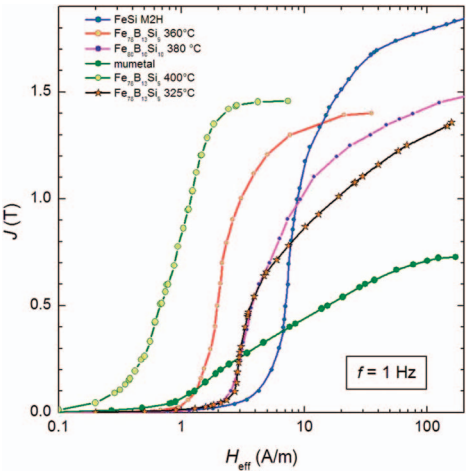

Fig. 3. Normal magnetization curves measured in Fe-B-Si amorphous alloys, mumetal, and GO Fe-Si strip samples.

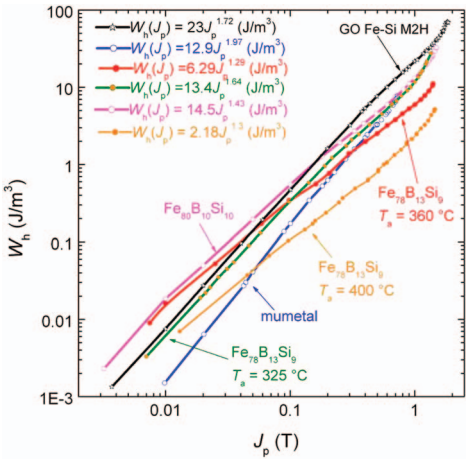

Fig. 4. Dependence of specific loss per cycle W on polarization J_p in quasistatic ($f = 1$ Hz) conditions. Power-law behavior ($W = kJ_p^n$) is verified for all materials.

obtained in the $Fe_{78}B_{13}Si_9$ strip field annealed at 360°C. The near-rectangular intrinsic hysteresis loop is retrieved from the measured loop by introducing the effective field

$$H_{\text{eff}} = H_a + H_d = H_a - (N_d/\mu_0)J, \qquad (1)$$

where H_a and H_d are the applied and demagnetizing fields, respectively, and N_d is the fluxmetric demagnetizing factor [26]. This correction can be done accurately because of the near-rectangular shape of the loop. It is remarkably found that N_d is proportional to the strip thickness.

In Fig. 2(Right), the major intrinsic hysteresis loops obtained in all the investigated materials are compared. The corresponding normal magnetization curves are shown in Fig. 3. Both figures put in evidence a substantial range of behaviors, with the $Fe_{78}B_{13}Si_9$ amorphous alloys exhibiting good versatility, in response to the specifically applied thermomagnetic treatment. Fig. 4 summarizes the dependence of the quasistatic energy loss per cycle and per unit volume W on the peak polarization J_p. A power law $W(J_p) \propto J_p^n$, with n ranging between 1.3 and 1.97, is verified to good approximation in all materials, but for J_p approaching the saturation polarization J_s. To evaluate the dissipative response of these materials and to find the strip assembly leading to maximum magnetic losses, under the boundary condition imposed by the practically available strip geometries, we need to know the dependence of the energy loss on the applied alternating field strength of peak value H_a, and we must accordingly translate the (W, J_p) behavior shown in Fig. 4 in the corresponding (W, H_a) behavior. This will obviously depend on the value of the demagnetizing coefficient N_d, that is, on the geometrical properties of the strips and their arrangement in the array. For any combination of H_a and N_d, the J_p value is thus found as the intercept of the normal magnetization curve with the demagnetizing (1), as in the example shown in Fig. 5, concerning two different field-strength values: $H_a = 2$ A/m, and $H_a = 20$ A/m. The (W, H_a) relationship is thus retrieved for any N_d value. Fig. 6 provides an example of the role of N_d in determining the (W, H_a) dependence on the investigated materials. It is apparent that a major effect brought about by the demagnetizing field is, beyond the obvious reduction of the magnetic loss for a same applied field H_a, a partial relaxation of the differences between different materials. The problem remains, in any case, of finding the strip arrangement leading to maximum losses under an as wide as possible range of applied field values.

IV. A PREDICTING APPROACH TO MAGNETIC LOSSES IN A STRIP ARRAY

Maximizing the magnetic losses of a strip array under given applied alternating field is a many-variable problem, with geometrical and intrinsic parameters playing a correlated role. Possible solutions additionally suffer from practical constraints imposed by the previously mentioned geometrical limitations of the samples. We propose here a predictive approach based on a simplified description of the strip-to-strip interaction by a dipolar model.

A. Cumulative Strip Array Demagnetizing Field

To start with, let us assume that the strips are uniformly magnetized (which cannot be the case, because they are not ellipsoids) and let us calculate the field that a strip of length $2l$, width w, and thickness d, located at the origin of coordinates applies at the center of an identical parallel strip nearby placed. The distance between the strip axes is $x = w + h$ and the magnetic pole charge at the strip ends is $q = Mwd$, if M is the material magnetization. With reference to Fig. 7, we can write for the dipolar field

$$|H_1| = |H_2| = (Mwd)/(4\pi r^2). \qquad (2)$$

The z component of the interaction field therefore is

$$H_z = 2H_1 \cos\theta = 2(Mwd/4\pi) \cdot l/(l^2 + x^2)^{3/2}. \qquad (3)$$

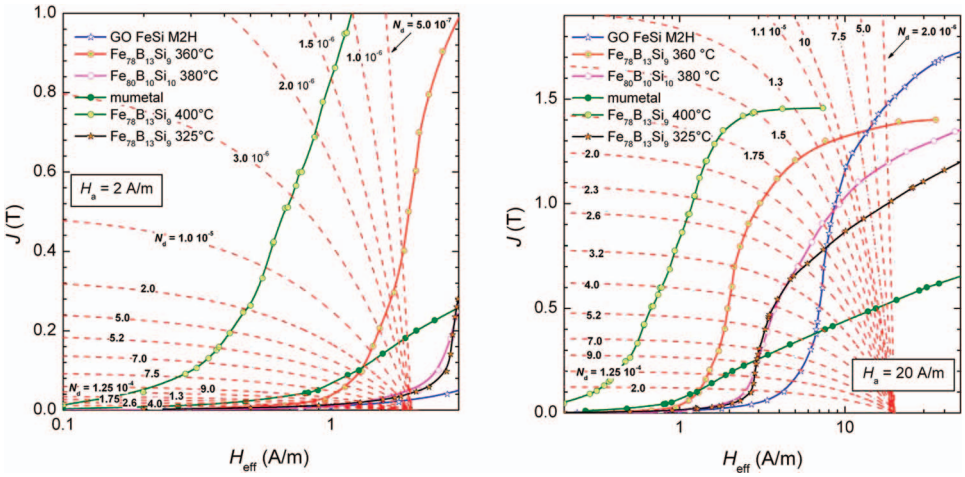

Fig. 5. Working points (H_a, J_p) of strip array for any given combination (H_a, N_d) are found as intercepts of demagnetizing curves of equation $H_{eff} = H_a - (N_d/\mu_0)J$ (dashed lines, N_d ranging between $5\cdot10^{-7}$ and $4\cdot10^{-4}$) with intrinsic normal magnetization curves (H_{eff}, J). Energy loss is then retrieved using experimental (W, J_p) relationship, shown in Fig. 4.

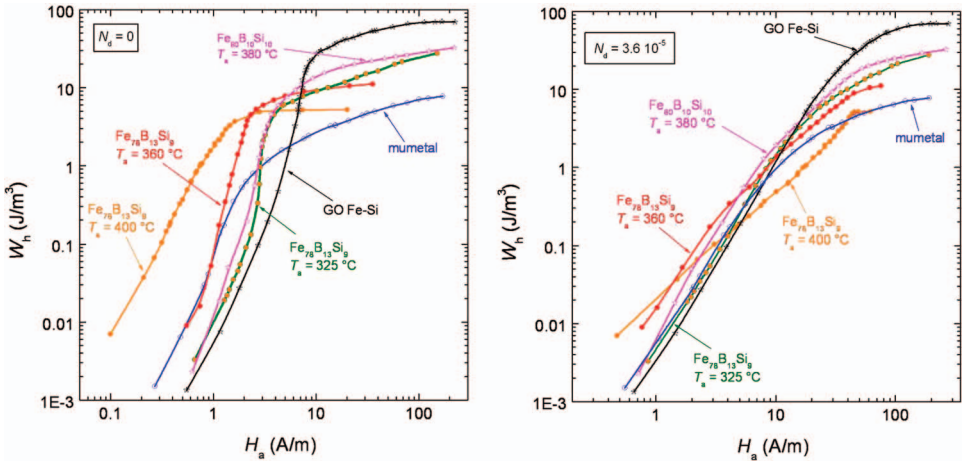

Fig. 6. Specific energy loss versus peak value of applied alternating field H_a (left) and role of demagnetizing field (right). Note that loss decrease brought about by demagnetizing effect undergiven applied field strength. Large differences in loss behaviors observed in different materials with $N_d = 0$ are partly relaxed when N_d attains values expected for actual strip arrays.

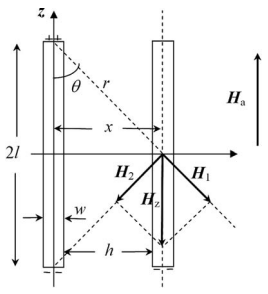

Fig. 7. Dipolar interaction between uniformly magnetized parallel strip samples. z component of interaction field has demagnetizing character, and resulting material behavior can be interpreted in terms of augmented demagnetizing factor.

A strip immersed in an array will be subjected, besides the applied field H_a and its own demagnetizing field H_{do}, to an additional demagnetizing field deriving from the dipolar interaction with all the other strips, according to (3). The bar suffering most the demagnetization effect is the one at the center of the strip array, and this can be taken as the worst case. One can thus write [see (4)] for the cumulative demagnetizing field acting on a strip at the center of an array made of $2N + 1$ identical strips of length $2l$ located at the coordinates x_i

$$H_d = H_{do} + (Mwd/\pi) \cdot \sum_{i=1}^{N} \frac{l}{(l^2 + x_i^2)^{3/2}}. \qquad (4)$$

But any strip, even when subjected to a uniform magnetic field H_a, is never uniformly magnetized, because the demagnetizing field cannot be uniform along the strip length. Equation (4) is, therefore, suitably generalized, with the introduction of parameters provided by the experiments. This is equivalently done in terms of a demagnetizing factor N_d, which, in view of the proportionality found between thickness d and H_d, can be normalized to unit strip thickness $n_d = N_d/d$. The augmented (cumulative) normalized demagnetizing factor

TABLE II
Experimental Constants A and B Used in the Evaluation by (5) of the Cumulative Demagnetization Coefficient of the Arrays Obtained with Strips (100 mm and 200 mm Long)

strip length	A	B
100 mm	$3.88{\cdot}10^{-4}$ m	$9.8{\cdot}10^{-3}$ m
200 mm	$1.10{\cdot}10^{-3}$ m	$2.4{\cdot}10^{-2}$ m

of the strip located at center of the array is then written as

$$n_{\mathrm{d,cumul}} = n_{\mathrm{do}} + 2Aw \cdot \sum_{i=1}^{N} \frac{1}{(B^2 + x_i^2)^{3/2}} \ [\mathrm{m}^{-1}], \quad (5)$$

where n_{do} is obtained by direct measurement of the hysteresis loop on the single strip (see Fig. 2a). For the 100-mm-long strips, we find near-linear increase of n_{do} with the strip width below about $w = 10$ mm. It is, in particular, $n_{\mathrm{do}} = 0.33\ \mathrm{m}^{-1}$, $1.77\ \mathrm{m}^{-1}$, $2.70\ \mathrm{m}^{-1}$ for $w = 1$ mm, 5.4 mm, and 10 mm, respectively. If longer or shorter strips are employed, it is observed that n_{do} scales with the length as $(2l)^{1.7}$, close to the standard results obtained for the fluxmetric demagnetizing factor in cylinders [21]. The constants A and B are determined by best fitting of the global demagnetizing factor $N_{\mathrm{d,cumul}}$ of the array versus the strip-to-strip distance h, as obtained by the measurement of the corresponding hysteresis loop. We have done this on an array (100 mm $\times$ 100 mm) made with $Fe_{78}B_{13}Si_9$ amorphous strips ($w = 5.4$ mm, $d = 20.3$ μm), annealed at 325°C, obtaining the data indicated inTable II. With the so-obtained values of the geometrical parameters A and B, we can, therefore, predict $N_{\mathrm{d,cumul}}$ for all arrays made with strips (100 mm long), whatever the material, the strip width, and the strip thickness. It is an acceptable approximation as the fluxmetric demagnetizing coefficient becomes material independent and the closest to the magnetometric demagnetizing coefficient when, like in the present alloys, the involved permeability is very high [21, 26]. Note that in doing so, we make the assumption that the array is sufficiently large to equalize to a good extent the behavior of all the strips so that the cumulative demagnetizing factor of the single strips in the array $n_{\mathrm{d,cumul}}$ and that of the whole array are approximately the same. Fig. 8 shows how the calculated $n_{\mathrm{d,cumul}}$ evolves with increasing the number of strips (that is, the width $2\times$ of the array) for different values of the strip-to-strip gap h (in this case, strips,100 mm long, 5.4 mm wide, and 20.3 μm thick, laid side-by-side at a distance $0 \le h \le 80$ mm). $n_{\mathrm{d,cumul}}$ saturates on reaching the array width 100 mm.

Calculated and measured behaviors of $N_{\mathrm{d,cumul}}$ versus h in an array (100 mm $\times$ 100 mm and 200 mm $\times$ 200 mm) are shown in Figs. 9 and 10, respectively. Although the demagnetizing factor of the single strip is retrieved for large h values, it is noted that on passing from the array of 100 mm $\times$ 100 mm to the array of 200 mm $\times$ 200 mm with adjacent ($h = 0$) strips of equal thickness, the expected reduction of $N_{\mathrm{d,cumul}}$ by about a factor two is experimentally verified.

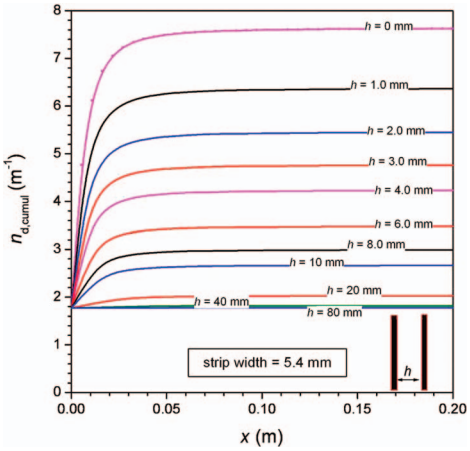

Fig. 8. Cumulative demagnetizing factor $n_{\mathrm{d,cumul}}$ of strip array, normalized to strip thickness d, calculated with (5) as function of array half-width x. Different curves refer to different values of strip-to-strip gap h.

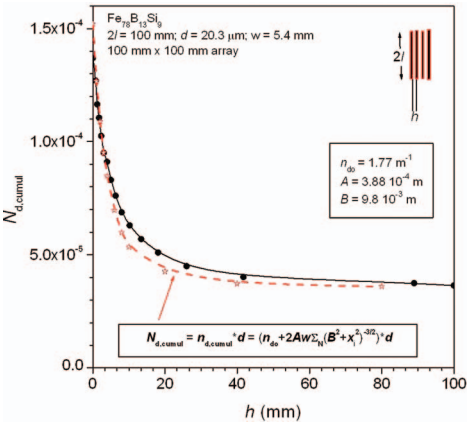

Fig. 9. Experimental dependence of global demagnetizing factor $N_{\mathrm{d,cumul}}$ of array (100 mm $\times$ 100 mm; full symbols) on strip-to-strip separation (open symbols) and its prediction by (5).

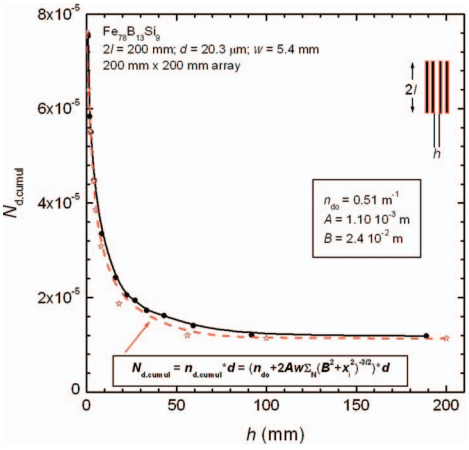

Fig. 10. As in Fig. 9, for array (200 mm $\times$ 200 mm).

B. Specific Energy Loss in a Uniformly Magnetized Strip Array

Having established the relationship between the geometrical properties of the strips, their configuration in the array and the related cumulative demagnetizing factor $N_{d,cumul}$, we can proceed to the calculation of the energy dissipated in the array for any value of the alternating applied field H_a. We ignore, for the moment, the actual decay of the magnetization value towards the strip ends, and we point to the prediction of the energy loss $W(0)$ at the array mid-cross section. Correction for the magnetization decay will be provided in the next Subsection IV C. It is an easy matter to retrieve, for all materials, the specific energy loss dependence on H_a. Starting from the known experimental intrinsic (H_{eff}, J_p) and (W, J_p) relationships (Figs. 3 and 4) and the demagnetizing (1), now written as $H_a = H_{eff} + (N_{d,cumul}/\mu_0)J_p$, the ($W$, H_a) behavior is obtained for any value of $N_{d,cumul}$. To this end, we follow the procedure described in Section III and exemplified in Fig. 5, where the working point (H_a, J_p) is obtained as the intercept of the normal magnetization curve $J_p(H_{eff})$ with the demagnetizing curve H_{eff} (J_p) $= H_a - (N_{d,cumul}/\mu_0)J_p$. The experimental energy loss per unit cycle and unit volume follows then by the experimental law $W(J_p(H_a)) = kJ_p{}^n$, where k is a material-dependent constant and n ranges between 1.3 and 1.97. With W expressed in joules per cubic meter, k oscillates between 2.18 and 23 in the investigated materials (see Fig. 4). The predicted energy loss per unit length of an array of parallel strips of length $2l$, width w and thickness d cyclically magnetized between $\pm J_p$ under a field oscillating between $\pm H_a$ becomes then

$$W_{ul}(0) = k(J_p(H_a))^n \cdot \frac{2lwd}{(w+h)}\ [\mathrm{J/m}]. \tag{6}$$

One may try to quantify the role of the effective permeability of the material at the working point $\mu_{eff} = (J_p/H_{eff}) = \mu_0\mu_{r,eff}$ on $W_{ul}(0)$. Because $J_p = \mu_{eff}H_{eff} = \mu_a H_a$, where $\mu_a = \mu_0\mu_{r,a}$ is the apparent permeability, we have $J_p = \mu_{eff}/(1 + N_{d,cumul}\mu_{r,eff}) \cdot H_a$. Substituting in (6) and using (5) with $x_i = i\cdot(w+h)$, we obtain the energy loss per unit array length

$$W_{ul}(0) = k \cdot \frac{2lwd}{w+h} \cdot \left[\frac{\mu_{eff} H_a}{1 + \mu_{r,eff}\left\{ N_{d0} + 2Awd \cdot \sum_{i=1}^{N} \left[B^2 + i^2 \cdot (w+h)^2 \right]^{-3/2} \right\}} \right]^n [\mathrm{J/m}], \tag{7}$$

showing the explicit dependence of the dissipated energy on the single isolated strip demagnetizing factor N_{d0}, the strip dimensions ($2l$, w, d), the strip-to-strip gap h, the total number of strips N, and the experimental geometric constants A and B, given in Table II. Equation (7) provides a valuable design tool, allowing one to evaluate the geometry of the strips and their arrangement (parameters

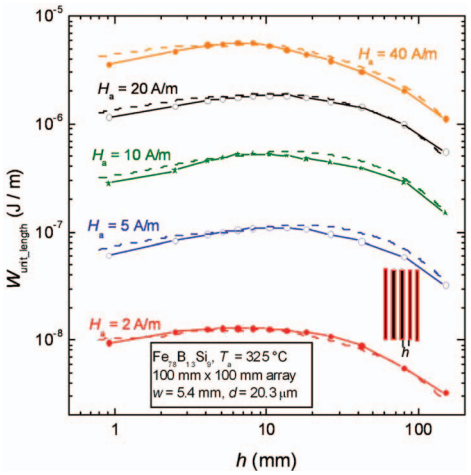

Fig. 11. Energy loss per unit length in array (100 mm × 100 mm) as function of strip-to-strip gap h. Array is obtained with $Fe_{78}B_{13}Si_9$ amorphous strips (5.4 mm wide and 20.3 μm thick), field-annealed at 325°C. Experimental W versus h behavior (symbols) is compared with prediction of model (dashed line).

$2l$, w, d, h), maximizing the loss for a given material and given intrinsic permeability. Fig. 11 shows a comparison between calculated and measured energy losses per unit array length versus h under five different values of the applied alternating field H_a, in the array (100 mm × 100 mm) made of $Fe_{78}B_{13}Si_9$ strips (5.4 mm wide and 20.3 μm thick), annealed at 325°C. Fig. 12 provides the same comparison for the array (200 mm × 200 mm).

It is observed that for any given H_a value, the energy loss attains a maximum value for an optimal strip-to-strip distance h typically ranging between 5 mm and 15 mm. It is, therefore, concluded that whatever the applied field, under certain conditions the dipolar interaction does not offset the advantage brought about by the increase of the sample mass and an optimal separation h between the strips can be found, for which the energy loss is, under given applied oscillating field, two to three times higher than that of the isolated strips.

Based on our predicting capability, we can perform a full analysis of the role of different strip geometries and different materials. Concerning the amorphous alloys, we know that they invariably come, after rapid solidification, as ribbons (18–25 μm thick). One might then look for increased dissipating volume by superposing two or more ribbons. The calculations show, however, in both arrays (100 mm × 100 mm and 200 mm × 200 mm) that the ensuing increase of the demagnetizing field leads to

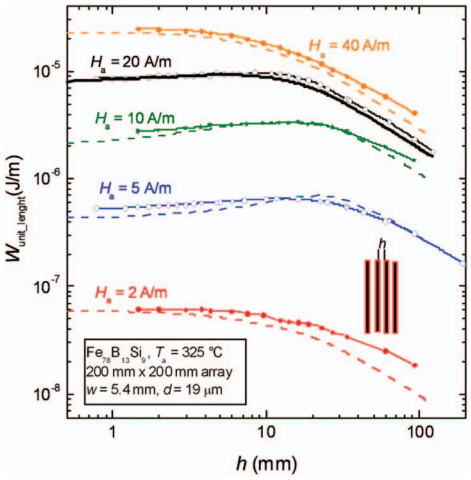

Fig. 12. As in Fig. 11, for array (200 mm × 200 mm).

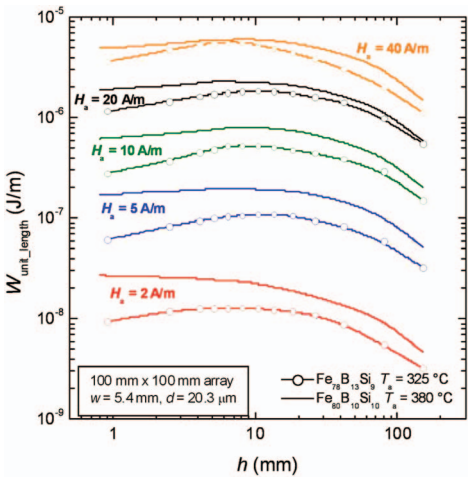

Fig. 13. Strip array (100 mm × 100 mm). Loss measured in array made of amorphous $Fe_{78}B_{13}Si_9$ ribbons annealed at 325°C (symbols) is compared with loss predicted for $Fe_{80}B_{10}Si_{10}$ ribbons annealed at 380°C (continuous lines).

decreased losses under any H_a value. It is concluded that arrays made of thinner strips combine reduced weight with increased loss.

As previously stressed, achieving very good soft magnetic behavior somewhat contrasts with the need for maximum dissipation. A good compromise can be achieved with Fe-based amorphous ribbons and their flexible response to magnetic annealing. We find, for example, that ribbons of composition $Fe_{80}B_{10}Si_{10}$, field-annealed at $T = 380$°C, have coercivity similar to the previous $Fe_{78}B_{13}Si_9$ ribbons annealed at 325°C but higher permeability (Fig. 2). This results, as illustrated in Fig. 13, into higher induction and higher losses under all H_a values. The amorphous $Fe_{80}B_{10}Si_{10}$ ribbons actually appear to provide, in general, the best dissipation performances of all the investigated materials, as put in evidence by the overall loss comparisons for the array (100 mm × 100 mm), shown in Fig. 14.

The amorphous alloys can always be treated in such a way as to provide superior performances with respect to the crystalline material under all applied field conditions. It is also realized that high strip thickness plays a detrimental role, as demonstrated by the loss prediction made for the cross-sectional area of the mumetal wires (1 mm × 1 mm).

C. Decay of the Magnetization Along the Strip Length

All the results and conclusions reported so far refer to the magnetic response of the material and the dissipating array across the strip mid-cross section. However, the magnetization in the strips decays from center to the ends because the demagnetizing field is not uniform along the strip length. It is, however, a simple matter to recover the loss pertaining to any cross-sectional area of the array, if a simple law of magnetization decay can be worked out. This law is found by experiments on the arrays, and, remarkably, we obtained that it is minimally dependent on the size of the array (either 100 mm × 100 mm or 200 mm × 200 mm), the distance between the strips h, and the strength of the applied oscillating field H_a. In addition, the decay experiments made on single strips show little differences among different materials. Fig. 15 shows the experimentally measured decay $J(y)/J(0)$ of the magnetization from center to end of strips in the two investigated arrays. It is minimally dependent on H_a and can be fitted to good extent, for an array of strips of length $2l$, with a power law of the type $J(y)/J(0) = 1 - 0.8 \cdot (y/l)^{2.5}$. This allows one to define an average polarization of the strip, useful for the numerical simulation of the strip magnetic dipole, as follows considering $l = 100$ mm:

$$\langle J \rangle = (1/l) \int_0^l J(y)dy = J(0)/l \times \int_0^l \left[1 - 0.8 \cdot (y/l)^{2.5}\right]dy = 0.7714 \cdot J(0). \quad (8)$$

As previously discussed, the energy loss depends on the peak magnetization value according to the power law $W = kJ_p{}^n$, with the constants k and n, depending on the type of material (see Fig. 4). We can, therefore, obtain, for any H_a value, the loss $\langle W \rangle$ on the whole array from knowledge of the previously calculated loss $W(0)$ upon its central cross section and the decay $J(y)/J(0)$ by making the integration

$$\langle W \rangle = (1/l) \int_0^l W(y)dy = W(J(0)) \cdot (1/l) \times \int_0^l \left[1 - 0.8 \cdot (y/l)^{2.5}\right]^n dy. \quad (9)$$

The experiments show $1.3 \leq n \leq 1.97$, the lower and upper limit belonging to the $Fe_{78}B_{13}Si_9$ amorphous ribbons annealed at $T = 400$°C and the mumetal strips, respectively. We see in the lower value of n a further advantage of the amorphous alloys. The integration provides, for example, $\langle W \rangle = 0.71\ W(J(0))$ for $Fe_{80}B_{10}Si_{10}$ ($n = 1.43$) and $\langle W \rangle = 0.65\ W(J(0))$ for mumetal ($n = 1.97$).

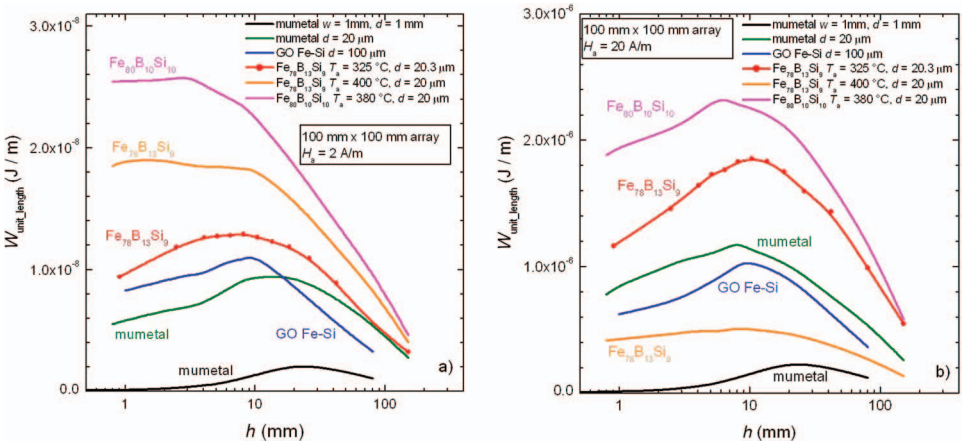

Fig. 14. 100 mm × 100 mm strip array. Predicted (continuous lines) and measured (symbols) energy losses versus strip arrangement in investigated materials under applied fields $H_a = 2$ A/m (a) and $H_a = 20$ A/m (b). Strip width $w = 5.4$ mm. Calculation for mumetal is made also for wires of cross-sectional area 1 mm × 1 mm.

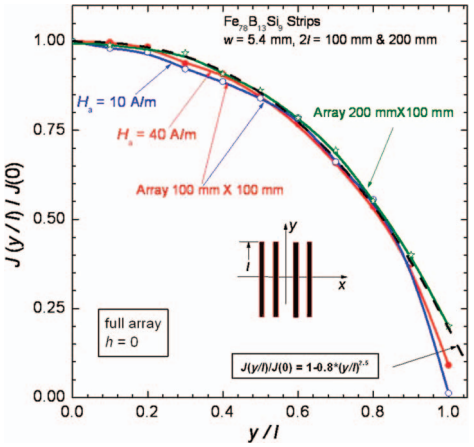

Fig. 15. Decay of reduced magnetization $J(x)/J(0)$ versus reduced distance x/l from center in strip array. It can be described according to power law $J(x)/J(0) = 1 - 0.8 \cdot (x/l)^{2.5}$.

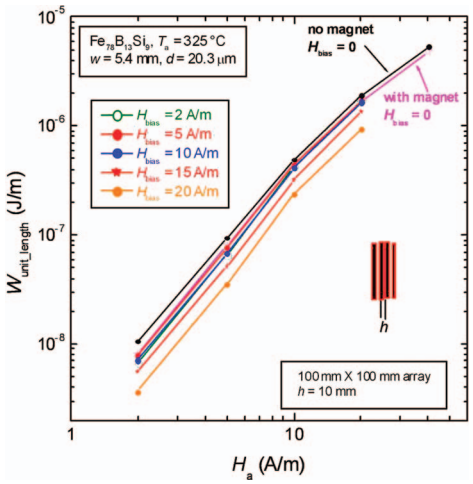

Fig. 16. Energy loss per unit array length versus applied alternating field measured in array (100 mm × 100 mm) made of $Fe_{78}B_{13}Si_9$ 20-μm-thick amorphous ribbons annealed at 325°C. Pivoting Nd-Fe-B cylindrical magnet of moment $m = 0.33$ Am^2 engenders slight reduction of loss figure. Additional presence of bias field H_{bias} gives rise to further decrease of loss.

V. THE PIVOTING MAGNET AND THE ROLE OF A BIAS FIELD

The maximum restoring torque in the Earth magnetic field can be obtained with minimum permanent magnet volume by choosing a rare-earth-based material, namely, Sm-Co or Nd-Fe-B compounds. A critical point in the use of this magnet is its symmetrical arrangement with respect to the plane of the array. The field lines emerging from the magnet must, in fact, cross the array orthogonal to the surface of the strips (N_d close to 1) to be ineffective on their magnetic state. Given the high value of the field generated by the permanent magnet, even a small misalignment can give rise to detrimental effects. We have investigated this problem by making the loss measurements under the usual range of H_a values with a Nd-Fe-B cylindrical magnet of length 20 mm and diameter 5 mm, symmetrically positioned across the optimal array configuration made with the 20.3-μm-thick and 5.4-mm-wide $Fe_{78}B_{13}Si_9$ ribbons annealed at 325°C (see Fig. 1). This magnet is endowed with a magnetic moment $m = 0.33$ Am^2, measured using the extraction method [26]. With such a configuration, we have further verified the role of a DC field H_{bias}, ranging between 2 A/m and 20 A/m, superposed to H_a. Fig. 16 shows how the (W, H_a) behavior is affected by the presence of the pivoting Nd-Fe-B magnet and the successive application of H_{bias}. Fig. 17 puts in evidence that the stray field generated by the permanent magnet makes the energy loss W in the array to decrease at most around 20% at very low H_a values. The addition of H_{bias} makes W decrease further, and for $H_{bias} > 20$ A/m, the loss reduction becomes larger than 50%. It is important to remark, however, that the experimental dependence of W on H_{bias} is found to be quite reversible in character. When dealing with magnetic hysteresis, one is indeed faced with history-dependent

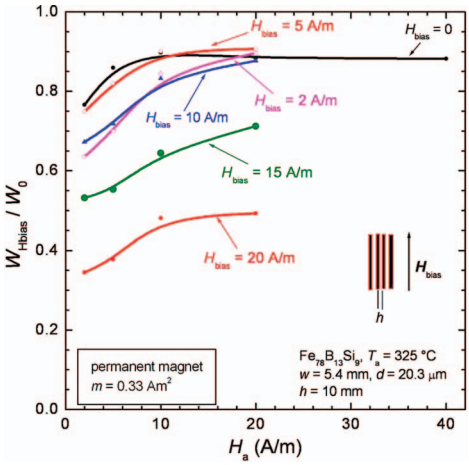

Fig. 17. Results given in Fig. 16 are represented in terms of ratio between loss measured with permanent magnet and bias field and loss obtained on unbiased array without magnet.

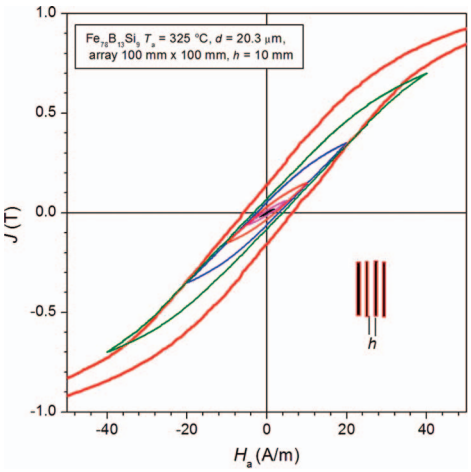

Fig. 18. Symmetric minor loops measured in array (100 mm × 100 mm) made of $Fe_{78}B_{13}Si_9$ 20-μm-thick amorphous ribbons annealed at 325°C placed at optimal distance $h = 10$ mm. Loops obtained with $H_a = 2$, 5, 10, 20, and 40 A/m are nested into major loop. Because of large demagnetizing effect, signaled by very low remanence value, near reversible dependence of loss on time variation of bias field is observed.

phenomena, and one should, in principle, approach the difficult problem of predicting the dissipation occurring in the magnetic array and the related frictional torque on the satellite following the complex evolution of the applied field versus time through a magnetic hysteresis model (e.g., the Preisach model). However, a close look at the hysteresis loops (J, H_a) measured on the arrays (Fig. 18) puts in evidence their pseudolinear behavior, where a very low remanence results from the large demagnetizing effect. We, therefore, expect that whatever the time history of H_{bias}, the measured loss will evolve with little or no hysteretic behavior [27].

VI. NUMERICAL SIMULATION OF THE PERFORMANCE IN ORBIT

The performance in orbit of magnetic damping systems based on the innovative Fe-B-Si amorphous strip arrays and the traditional mumetal strips are analyzed by numerical simulations, based on the measured hysteresis loop and energy dissipation evaluation discussed in Section IV. Permeable rods/strips onboard passively stabilized spacecrafts are exposed to irregular and nonsymmetric magnetizing fields. Accurate numerical prediction of their behavior can be built based on the Preisach model for magnetic hysteresis, whose application in satellite permeable rods is discussed, for example, in [28]. This approach is quite involved and computation intensive, therefore, not particularly suited for long-term attitude motion numerical propagation. A simplified model has been proposed in [24] and successfully applied for example in [17, 18, 29, 30]. This model has been recently elaborated further, leading to an analytical solution for the hysteresis curves, given an initial condition [14]. Taking advantage of the increased accuracy and related savings in computational burden, this solution was used in setting up the numerical simulations for the study cases analyzed in this section.

We consider a 1U CubeSat, which is a cubic-shaped nanospacecraft, with 10-cm sides and 1-kg weight. Due to the particular implementation of nanosatellite dispensers in multiple spacecraft launches performed by CubeSats, the satellite motion after separation from the launcher assumes an unpredictable initial attitude and angular velocity [31, 32]. Typically, a quite large initial angular rate, as high as 30 deg/s can be expected [14], with no preferential direction. The motion typically observed in passive magnetic attitude stabilization systems is a fast motion of the magnet axis with respect to the magnetic field, with large energy dissipation in the bars. When the initial kinetic energy is damped out, the magnet locks to the local magnetic field and starts oscillating in a way similar to a compass needle. This oscillatory motion is forced by the moving local magnetic field, rotating at about two revolutions per orbit in subpolar orbits. Whereas energy damping is quite fast in the rotation regime, in which the maximum magnetic field excursion is experienced by the permeable rods, the energy damping becomes slower when the satellite locks with the local magnetic field and the permeable rods see a very low amplitude variation of the magnetizing field. We will refer to these kinds of motions as a rotation regime and oscillation regime, respectively. The performance of the passive magnetic control system can be measured by the time needed to lock with the magnetic field and by the amplitude of the residual oscillation after final attitude stabilization is reached. For the first regime, an analytic approximate model based on averaging technique has been developed in [1], resulting in a linear decay of the angular velocity with time. This model remains valid until the angular velocity is high enough for the averaging simplification to hold. For the second regime, where hysteresis loops may not be symmetrical and the magnetizing field amplitude can be highly irregular over time, one must rely on numerical simulations.

Two magnetic damping systems are analyzed: one based on the innovative Fe-B-Si amorphous strip arrays

TABLE III
Parameters of the Strip Array Considered in the Numerical Simulation

Material	h (mm)	$N_{d,cumul}$	H_c (A/m)	J_p (T)	J_r (T)
$Fe_{80}B_{10}Si_{10}$	5	$6.8{\cdot}10^{-5}$	3.5	1.2·0.77	0.065
Mumetal	24	$2.0{\cdot}10^{-3}$	3.5	0.6·0.77	$2.2{\cdot}10^{-3}$

and one based on traditional cross-sectional mumetal strips (1 mm $\times$ 1 mm). Both systems are made of 100-mm-long strips, as dictated by the satellite size. The experimental results in Section IV showed that the lowest strip thickness should be taken, as allowed by the technological manufacturing process, whereas an optimal distance among the strips can be found, which maximizes the overall system magnetic loss. According to Fig. 14, the maximum energy dissipation per cycle is obtained using 20-μm-thick, 5-mm-wide $Fe_{80}B_{10}Si_{10}$ strips, with distance between the strips h in the order of 5 mm. Hence, taking into account that the maximum space allowed for the strips in a 1U CubeSat is 100 mm, we selected a system of 10 equally spaced strips, with a centerline distance of 10 mm. This was selected as the best performing magnetic damping systems in both the rotations ($H_a = 20$ A/m) and oscillations ($H_a = 2$ A/m) regimes. Concerning the mumetal strips (1 mm $\times$ 1 mm), Fig. 14 shows that the maximum dissipation is obtained for $h = 25$ mm. Hence, we selected a system of four bars, to cover the allowed 100-mm space. The synthetic magnetic parameters necessary to simulate the strip magnetic history, according to the model proposed in [24], are those pertaining to the major hysteresis loop: coercive field H_c, peak polarization value J_p, and polarization at remanence J_r. The value of the coercive field is directly obtained from Fig. 2. The peak value of the magnetic polarization can be determined multiplying the value obtained in Fig. 2 by the factor 0.77 obtained in (8), taking into account the polarization decay along the strip length. The remanence can be obtained applying the cumulative demagnetization factor $N_{d,cumul}$ from (5), or directly from Fig. 9 for the 100-mm-long strips, to the intrinsic hysteresis loops in Fig. 2. These values are reported inTable III.

The results of numerical simulation for a 1U CubeSat with spherically symmetrical mass distribution and moments of inertia 0.002 kgm^2 are shown in Figs. 19–22. The satellite is assumed as a rigid body moving under the effect of all the relevant environmental torques, including aerodynamic, gravity gradient, and magnetic torque. The distance between the center of pressure and the center of mass is assumed as 2 mm. The simulations are related to a circular Sun-synchronous orbit at 800-km altitude, representative of typical small satellite missions in high inclination orbits. The Earth's magnetic field model is a 10th-order International Geomagnetic Reference Field [33]. The passive magnetic attitude stabilization consists of a pivoting permanent magnet of magnetic moment $m = 0.33$ Am^2 and two orthogonal arrays of strips in the plane orthogonal to the permanent magnet, as shown in

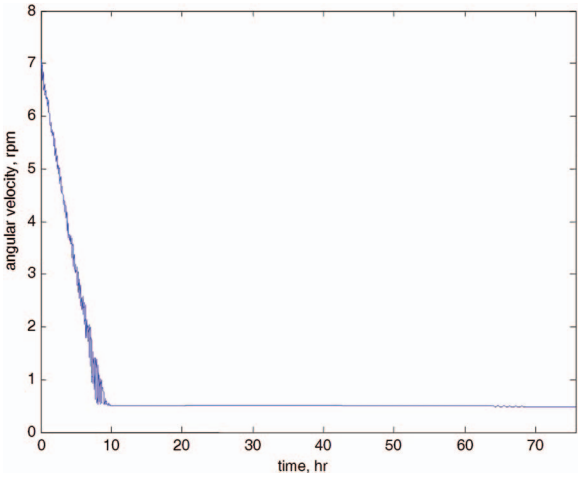

Fig. 19. Numerical simulation of angular velocity after separation from launcher, $Fe_{80}B_{10}Si_{10}$ strips.

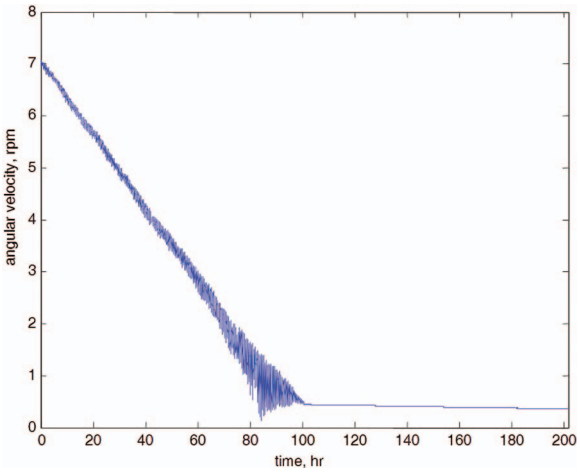

Fig. 20. Numerical simulation of angular velocity after separation from launcher, (1 mm $\times$ 1 mm) mumetal strips.

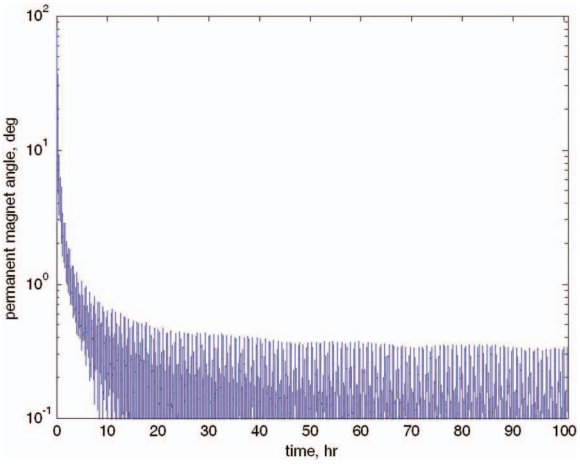

Fig. 21. Angle between permanent magnet and local Earth's magnetic field in oscillation regime, $Fe_{80}B_{10}Si_{10}$ strips.

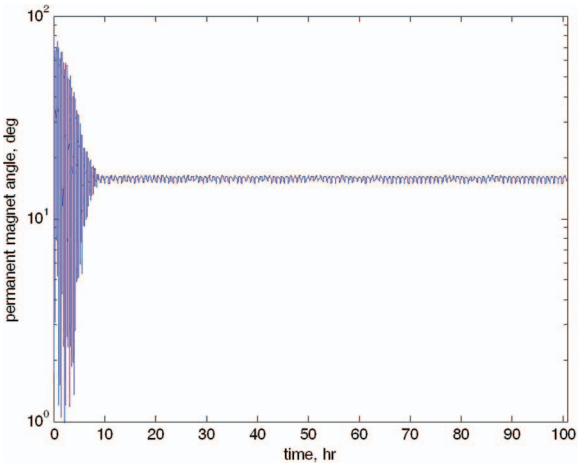

Fig. 22. Angle between permanent magnet and local Earth's magnetic field in oscillation regime, mumetal strips.

Fig. 1. The value of the onboard magnetic dipole was chosen based on the typical values of commercially available Nd-Fe-B magnets, verifying that no resonance conditions occur due to the coupling of attitude and orbital motion, as described in [15–18]. In the numerical simulations presented in Figs. 19–22, we assume an initial spin rate of 5 rpm along the two body axes orthogonal to the magnet. In this way, no relative motion is present at the initial time between the permeable rods and the magnetic field, hence, with minimum dissipative effects. At the same time, the magnet is moving quickly with respect to its target attitude, which is the local magnetic field, assumed as a worst-case test condition.

The analysis of the damping performance in the rotations regime can be effectively summarized by the modulus of the angular velocity, shown in Figs. 19 and 20 for the $Fe_{80}B_{10}Si_{10}$ and mumetal systems, respectively, during a typical rotation motion after separation from the CubeSat dispenser. In both cases, we observe a linear decrease of the angular velocity, as predicted in [1]. This behavior of the angular velocity damping in the rotations regime was largely expected. The superior performance of $Fe_{80}B_{10}Si_{10}$ strips descends from the larger dissipated energy per cycle exhibited by these materials, as discussed in previous sections. The performance of the two systems in the oscillations regime is shown in Figs. 21 and 22, where the angle between the onboard permanent magnet and the local Earth's magnetic field is plotted, starting from the initial value of 80°. The time needed to damp out oscillations is about 10 h in both cases. The residual oscillation amplitude is below half a degree for the amorphous alloy strips, whereas it amounts to about 15° for mumetal strips. The superior performance of amorphous strips is apparent.

We note that the total amorphous ribbons volume amounts to 100 mm^3 and the volume of the mumetal strips to 400 mm^3. Adding more volume to the mumetal strips would not improve their performance; hence, the amorphous ribbon strips combine increased performance with reduced volume and weight.

VII. CONCLUSIONS

We propose amorphous Fe-B-Si alloys as innovative soft magnetic materials for magnetic damping systems in passively stabilized nanospacecraft. The damping system consists of a planar array of mutually interacting soft magnetic strips. They have been characterized by an extensive experimental campaign in the whole range of magnetic fields expected for an orbiting device, comparing the energy dissipation performance of several magnetic materials and geometric configurations. A synthetic model of the magnetic properties of the strip array was developed, in which the strip-to-strip dipolar interaction is analytically taken into account by means of a simple Coulombian formulation. The demagnetizing effect is described by a cumulative demagnetization factor for the overall strip array, depending on two experimental parameters, regardless of the strip material. Hence, the loss in the strip array can be predicted from knowledge of the intrinsic magnetic properties of the employed soft magnets (i.e., normal magnetization curve and quasistatic energy loss versus peak polarization) and two experimental parameters. We provide such parameters for 100-mm- and 200-mm-long strips. Experimental results and predictions show that for a given material magnetic properties, an optimal configuration of the strip array exists, which leads to maximum energy dissipation. It is, therefore, concluded that the mutual strip interaction, when the bars come too close each other, cancels out the potential dissipation given by the additional strips. Experiments and predictions also show that arrays made of thinner strips combine reduced weight with increased loss. The magnetic damping system design process is described in the paper, showing how, depending on the material magnetic properties, the optimal strip distance is selected. For example, we show that the best performance of the amorphous array is obtained for a centerline distance among the strips of 10 mm, whereas for the conventional mumetal bars (1 mm $\times$ 1 mm), it is 25 mm. The expected performance in orbit of innovative Fe-B-Si ribbons and conventional mumetal bars (1 mm $\times$ 1 mm) under the effect of the irregular spacecraft attitude motion was evaluated by numerical simulation. The results confirm the ground testing data, with superior energy damping performance of the amorphous ribbons with respect to mumetal wires both in the rotation and oscillation regimes, respectively, experienced by the satellite after initial release in orbit and after acquisition of the stabilized attitude motion.

REFERENCES

[1] Fischell, R. E.
Magnetic damping of the angular motion of Earth satellites.
ARS Journal, **31** (1961), 1210–1217.

[2] Mesch, F.
Magnetic components for the attitude control of space vehicles.

IEEE Transactions on Magnetics, **5**, 2 (Mar. 1969), 586–592.

[3] Herzl, G. G.
Passive Gravity Gradient Libration Dampers, Vol. 3. Palo Alto, CA: Lockheed Missiles & Space Company, 1970.

[4] Heidt, H., Puig-Suari, J., Moore, A. S., Nakasuka, S., and Twiggs, R. J.
CubeSat: a new generation of picosatellite for education and industry low-cost space experimentation.
Presented at the *AIAA/USU Conference on Small Satellites*, Logan, UT, Aug. 21–24, 2000.

[5] Toorian, A., Diaz, K., and Lee S.
The CubeSat approach to space access.
In *Proceedings of the 2008 IEEE Aerospace Conference*, Big Sky, MT, Mar. 2008, 1–14.

[6] Graziani, F., Piergentili, F., and Santoni, F.
A space standards application to university-class microsatellites: the UNISAT experience.
Acta Astronautica, **66**, 9–10 (May–June 2010), 1534–1543.

[7] Alminde, L., and Laursen, K. K.
A strategic approach to developing space capabilities using Cubesat technology.
In *Proceedings of the 4th International Conference on Recent Advances in Space Technologies*, Istanbul, Turkey, June 2009, 43–47.

[8] J. Piattoni, J., Candini, G. P., Pezzi, G., Santoni, F., and Piergentili, F.
Plastic Cubesat: an innovative and low-cost way to perform applied space research and hands-on education.
Acta Astronautica, **81**, 2 (Dec. 2012), 419–429.

[9] Candini, G. P., Piergentili, F., and Santoni, F.
Miniaturized attitude control system for nanosatellites.
Acta Astronautica, **81**, 1 (2012), 325–334.

[10] Santoni, F.
Risk management for microsatellite design.
Acta Astronautica, **54**, 3 (Feb. 2004), 221–228.

[11] Santoni, F., and Piergentili, F.
UNISAT-3 attitude determination using solar panel and magnetometer data.
Presented at the *56th International Astronautical Congress*, Fukuoka, Japan, Oct. 17–21, 2005.

[12] Hamann, R. J., Bouwmeester, J., and Brouwer, G. F.
Delfi-C3 preliminary mission results.
Presented at the *23rd Annual AIAA/USU Conference on Small Satellites*, Logan, UT, Aug. 10–13, 2009.

[13] Poppenk, F. M., and Amini, R.
Delfi-C3 control system development and verification.
Presented at the *57th International Astronautical Congress*, Valencia, Spain, Oct. 2–6, 2006.

[14] Burton, R., Starek, J., and Rock, S.
A New Method for Simulating the Attitude Dynamics of Passively Magnetically Stabilized Spacecraft. San Diego, CA: Univelt, 2012.

[15] Ovchinnikov, M. Y., and V. I. Penkov, V. I.
Passive magnetic attitude control system for the *Munin* nanosatellite.
Cosmic Research, **40**, 2 (2002), 142–156.

[16] Rauschenbakh, B. V., Ovchinnikov, M., and McKenna-Lawlor, S.
Essential Spaceflight Dynamics and Magnetospherics, Vol. 15, Dordrecht, The Netherlands: Kluwer Academic Publishers, 2002.

[17] Santoni, F., and Zelli, M.
Passive magnetic attitude stabilization of the UNISAT-4 microsatellite.
Acta Astronautica, **65** (Sep.–Oct, 2009), 792–803.

[18] Battagliere, M. L., Santoni, F., Piergentili, F., Ovchinnikov, M., and Graziani, F.
Passive magnetic attitude stabilization system of the EduSAT micro satellite.
Journal of Aerospace Engineering, **224**, 10 (2010), 1097–1106.

[19] Gluck, R., and Wong, A.
Inline hybrid computer for simulation of passively stabilized satellites.
Journal of Spacecraft and Rockets, **6**, 7 (1969), 812–818.

[20] Sato, M., and Ishii, Y.
Simple and approximate expressions of demagnetizing factors of uniformly magnetized rectangular rod and cylinder.
Journal of Applied Physics, **66**, 2 (1989), 983–985.

[21] Chen, D. X., Brug, J. A., and Goldfarb, R. B.
Demagnetizing factors for cylinders.
IEEE Transactions on Magnetics, **27** (1991), 3601–3619.

[22] Aharoni, A.
Demagnetizing factors for rectangular ferromagnetic prisms.
Journal of Applied Physics, **83**, 6 (1998), 13432–3434.

[23] Ovchinnikov, M.
Attitude dynamics of a small-sized satellite equipped with hysteresis damper.
In *Proceedings of the 1st IAA Conference on Dynamics and Control of Space Systems*, Porto, Portugal, Mar. 19–21, 2012, 311–330.

[24] Flatley, T. W., and Henretty, D. A.
A magnetic hysteresis model.
In *Proceedings of the Flight Mechanics/Estimation Theory Symposium*, Greenbelt, MD, May 1995, 405–415.

[25] Battagliere, M. L., Fiorillo, F., Ferrara, E., and Santoni, F.
Permeable rods ground testing system for Cubesat angular velocity and residual osscillations damping.
In *Proceedings of the 61st International Astronautical Congress*, Prague, Czech Republic, Sep. 27–Oct. 1, 2010.

[26] Fiorillo, F.
Measurement and Characterization of Magnetic Materials. San Diego, CA: Elsevier-Academic Press, 2004, p. 409.

[27] Fiorillo, F., Santoni, F., Ferrara, E., Battagliere, M. L., Bottauscio, O., and Graziani, F.
Soft magnets for passive attitude stabilization of small satellites.
IEEE Transactions on Magnetics, **46**, 2 (Feb. 2010), 670–673.

[28] Whisnant, J. M., Anand, D. K., Pisacane, V. L., and Sturmanis, M.
Dynamic modeling of magnetic hysteresis.
Journal of Spacecraft and Rockets, **7**, 6 (June 1970).

[29] Kumar, R. R., Heck, M. L., and Mazanek, D. D.
Simulation and Shuttle Hitchhiker validation of passive satellite aerostabilization.
Journal of Spacecraft and Rockets, **32** (Sep. 1995), 806–811.

[30] Park, G., Seagraves, S., and McClamroch, N. H. A
dynamic model of a passive magnetic attitude control system for the RAX nanosatellite,
In *Proceedings of the AIAA Guidance, Navigation, and Control Conference*, Toronto, Ontario, Canada Aug. 2–5, 2010.

[31] Nason, I., Puig-Suari, J., and Twiggs, R.
Development of a family of picosatellite deployers based on the CubeSat standard.
In *Proceedings of the 2002 IEEE Aerospace Conference*, Big Sky, MT, 2002, 457–464.

[32] Santoni, F., Piergentili, F., and Ravaglia, R.
Nanosatellite cluster launch collision analysis.
Journal of Aerospace Engineering, **26**, 3 (July 2013), 618–627.

[33] Finlay, C. C., Maus, S., Beggan, C. D., Bondar, T. N., Chambodut, A.
International Geomagnetic Reference Field: the eleventh generation.
Geophysical Journal International, **83** (2010), 1216–1230.

Fabio Santoni received the Dr. Eng. degree in 1992 in aeronautical engineering (cum laude) and the Ph.D. degree in aerospace engineering in 1996, both from University of Rome "La Sapienza." He is presently associate professor in Aerospace Systems at University of Rome "La Sapienza," where he established the Aerospace Systems Laboratory.

Maria Libera Battagliere has a Ph.D. degree in aerospace engineering. Her main research fields are the design and manufacturing of payloads for space education microsatellites, Earth observation, and passive attitude control systems. She is, at the present, employed at the Italian Space Agency in the framework of Cosmo SkyMed program.

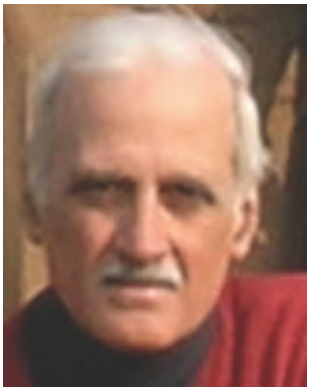

Fausto Fiorillo was Research Director at the Istituto Nazionale di Ricerca Metrologica (INRIM) in Torino (formerly Istituto Elettrotecnico Nazionale Galileo Ferraris) before his retirement in 2012. At present, he is pursuing his research studies in magnetism at INRIM as an associate scientist. His scientific work and interests have been mainly devoted to the properties of magnetic materials and their measurement, with special focus on magnetization process and losses.

He authored/coauthored some 190 peer-reviewed publications in international scientific journals, review monographs, and chapters on international series on magnetic materials (Hirsch-factor 21, ISI Thomson Reuters). He is the author of the comprehensive treatise *Measurement and Characterization of Magnetic Materials* (10 chapters and 647 pages), published by Academic Press-Elsevier, December 2004.

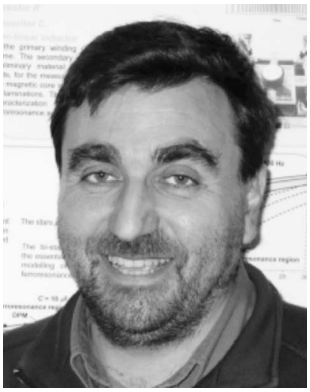

Enzo Ferrara chemist, is research scientist at the Istituto Nazionale di Ricerca Metrologica, Torino, Italy.